Title

Nf1-Mutant Tumors Undergo Transcriptome and Kinome Remodeling after Inhibition of either mTOR or MEK

Journal

Molecular Cancer Therapeutics, 19(11)

ISSN

1535-7163

Authors

Pucciarelli, Daniela
Angus, Steven P
Huang, Benjamin
et al.

Publication Date

2020-11-01

DOI

10.1158/1535-7163.mct-19-1017

Peer reviewed

HHS Public Access

Author manuscript

Mol Cancer Ther. Author manuscript; available in PMC 2021 August 14.

Published in final edited form as:

Mol Cancer Ther. 2020 November ; 19(11): 2382–2395. doi:10.1158/1535-7163.MCT-19-1017.

Nf1 mutant tumors undergo transcriptome and kinome re-modeling after inhibition of either mTOR or MEK

Daniela Pucciarelli[1], **Steven P. Angus**[2,*], **Benjamin Huang**[3], **Chi Zhang**[4], **Hiroki J. Nakaoka**[1], **Ganesh Krishnamurthi**[1], **Sourav Bandyopadhyay**[5], **D. Wade Clapp**[4], **Kevin Shannon**[3], **Gary L. Johnson**[2], **Jean L. Nakamura**[1]

[1]Department of Radiation Oncology, University of California San Francisco, San Francisco, California

[2]Department of Pharmacology, University of North Carolina School of Medicine, Chapel Hill, North Carolina

[3]Department of Pediatrics, University of California San Francisco, San Francisco, California

[4]Department of Pediatrics, Indiana University, Indianapolis, Indiana

[5]Department of Bioengineering & Therapeutic Sciences, University of California San Francisco, San Francisco, California

Abstract

Loss of the tumor suppressor *NF1* leads to activation of RAS effector pathways, which are therapeutically targeted by inhibition of mTOR (mTORi) or MEK (MEKi). However, therapeutic inhibition of RAS effectors leads to the development of drug resistance and ultimately disease progression. To investigate molecular signatures in the context of *NF1* loss and subsequent acquired drug resistance we analyzed the exomes, transcriptomes and kinomes of *Nf1* mutant mouse tumor cell lines and derivatives of these lines that acquired resistance to either MEKi or mTORi. Biochemical comparisons of this unique panel of tumor cells, all of which arose in $Nf1^{+/-}$ mice, indicate that loss of heterozygosity of *Nf1* as an initial genetic event does not confer a common biochemical signature or response to kinase inhibition. While acquired drug resistance by *Nf1* mutant tumor cells was accompanied by altered kinomes and irreversibly altered transcriptomes, functionally in multiple *Nf1* mutant tumor cell lines MEKi-resistance was a stable phenotype, in contrast to mTORi-resistance, which was reversible. Collectively these findings demonstrate that *Nf1* mutant tumors represent a heterogeneous group biochemically and undergo broader remodeling of kinome activity and gene expression in response to targeted kinase inhibition.

Corresponding Author: Jean Nakamura, University of California, San Francisco Helen Diller Family Cancer Research Center 1450 Third Street, Box 3112, San Francisco, California, USA 94158 Jean.Nakamura@ucsf.edu; phone (415) 514-4997; fax (415) 353-8679.
*Present address: Departments of Pediatrics and Pharmacology & Toxicology, Indiana University School of Medicine, Indianapolis, IN

Conflicts of Interest: The authors declare no potential conflicts of interest.

Keywords

Neurofibromatosis I; RAS signaling; MEK and mTOR inhibition; transcriptome; kinome; exome

INTRODUCTION

Neurofibromatosis I (NF1) syndrome is a tumor predisposition syndrome that is caused by a germline mutation in the *NF1* gene. Tumorigenesis in the setting of germline *NF1* heterozygosity is characterized by loss of the wildtype *NF1* allele, resulting in nullizygosity. This central event in *NF1*-mediated tumorigenesis leads to hyperactivation of RAS signaling pathways (1).

Downstream of RAS, activated RAF-MEK-ERK and PI3K-AKT-mTOR pathways are pharmacologically inhibited for therapy, the most clinically validated targets being MEK or mTOR. Unfortunately, single target inhibition leads to compensatory feedback and subsequently the development of drug resistance. For example, MEK inhibition leads to an increase in AKT and mTOR activity by decreasing IRS-1 phosphorylation in a variety of tumor types, including lung, pancreas, colon, bladder and prostate (1, 2), whereas in breast cancer, MEK inhibition is associated with enhanced EGFR/HER2 signaling and activation of AKT (3). Such differences in kinase signaling profile and therapeutic response have been linked to organ or context-dependence (4).

Although Neurofibromatosis type 1 is classified as a subtype of RASopathies, a group of clinical syndromes caused by hyperactivation of the RAS/MAPK pathway, the NF1 syndrome is notable for the phenotypic variation observed in affected individuals (5, 6). This clinical variation suggests significant heterogeneity in the mechanism by which *NF1* loss promotes multi-organ disease features.

Kinase inhibition is an important therapeutic strategy in the management of neoplasms in NF1. MAPK pathway inhibition suppresses the growth of malignant peripheral nerve sheath tumors (MPNSTs) (7, 8) as well as the development of hematopoietic malignancy in *Nf1* mutant mice (9). The MEK inhibitor selumetinib was recently identified as the first active therapy for plexiform neurofibromas in NF1, and the FDA granted breakthrough therapy designation for this therapy (10). Combined mTORC1 and MEK inhibition is proposed to be superior to inhibition of either of these effectors alone in the treatment of MPNSTs (11). However, questions remain concerning optimal strategies against RAS pathway activation in many *NF1* mutant malignancies, with novel therapeutic approaches yielding mixed responses in clinical trials (12). One potential explanation for the apparent mixed response in *NF1* mutant tumors may be that *NF1* loss, compared to mutant hyperactive RAS, is a weak driver of tumorigenesis. As such, cooperating events that promote tumorigenesis may also form the basis for heterogeneous clinical responses. The signaling framework also likely influences the mechanisms underlying acquired drug resistance, which can evolve from secondary mutations as well as alternate mechanisms of kinase pathway activation.

We sought to determine whether neoplasms linked by a common pathogenetic mechanism (loss of heterozygosity of *Nf1*, as occurs in Neurofibromatosis I syndrome) demonstrate

shared or divergent signaling features with functional and therapeutically significant consequences. In the context of a germline-mediated genetic syndrome such as NF1, in which multiple neoplasms may arise but are driven by a common initial genetic lesion, identifying shared biochemical and genetic alterations may point to therapeutic strategies with broader efficacy. Conversely, elucidating the mechanisms of divergent therapeutic responses should inform and predict patterns of treatment failure and the development of drug resistance.

In prior work, we generated mouse models of *Nf1*-driven tumorigenesis in which we mutagenized *Nf1* heterozygous mice with radiation, recapitulating the susceptibility of patients with NF1 to radiation-induced cancers (13, 14). These mouse models produced multiple diverse *Nf1* mutant tumor histologies (sarcomas and carcinomas) and associated cell lines that were universally characterized by *Nf1* nullizygosity (14, 15). Here, we derived MEKi or mTORi resistant *Nf1* mutant tumor cell lines by continuous exposure to the MEK inhibitor PD0325901 (PD901) or the mTOR inhibitor RAD001, then compared transcriptome and kinome profiles of these cells to parental cells. These studies identify stably acquired molecular signatures in the setting of drug resistance and suggest potential treatment strategies in the *Nf1* malignancy context.

MATERIALS AND METHODS

Cell lines, culture conditions and inhibitors

Cell lines, established from tumors arising in irradiated $Nf1^{+/-}$ F1 mice (17). Early passage stocks were established for all cell lines and experimental cells were drawn from these stocks approximately every twenty to thirty passages. Mycoplasma testing was done approximately yearly. Inhibitors were purchased from Selleck Chemicals (PD0325901 S1036, Everolimus (RAD001) S1120, Dactolisib (BEZ235) S1009, PD184352 (CI-1040) S1020, Torkinib (PP242) S2218, PIK-75 HCl S1205, Tozasertib (VX680) S1048, Barasertil (AZD1152) S1147, Alisertib (MLN8237) S1133, Binimetinib (MEK162) S7007, Trametinib (GSK1120212) S2673, Rapamycin (Sirolimus) S1039). Drug-resistant cell lines 989 PD_R, 989 RAD_R, 881 PD_R and 881 RAD_R were derived from each original parental cell line by continuous exposure to PD0325901 or RAD001. Cell lines 989 and 881 were exposed to increasing concentrations (from 25 nM to 500 nM) of PD0325901 or RAD001 for six months. Resistant cell lines were continuously maintained in medium supplemented with inhibitor. For drug washout experiments, cells were washed twice with PBS, inhibitors were withdrawn for 12 days and further analyses performed.

Validation sequencing

Genomic DNA was extracted from parental and resistant cell lines and amplified by PCR utilizing custom primers (Supplementary Table 2) targeting exons 2 and/or 3 of murine *Hras, Nras and Kras*.

Ras Activation Assays

After 24 hours of serum starvation, 50–60% confluent cells were stimulated for 0, 5, 30 and 60 minutes with medium supplied with 10% FBS, harvested and protein lysates

were collected. RAS-GTP levels were assessed using the Ras Pull-down Activation Assay Biochem Kit according to the manufacturer's protocol (Cytoskeleton).

Proliferation assay

Cell proliferation was assessed by a colorimetric MTS assay according to the manufacturer's instructions (Cell Titer 96 Aqueous One Solution Cell Proliferation Assay, Promega). Cells seeded in 96 well plates were treated with different inhibitors and cell viability was measured after 72 hours.

Sample Preparation for Multiplex Inhibitor Beads/Mass Spectrometry and RNA/DNA Sequencing

Parental and resistant cell lines were grown to a confluence of 70%. Parental cell lines were treated with 500nM PD0325901 or RAD001 for 24 hour. Washed cell lines were lysed in MIB lysis buffer (50 mM HEPES, 150 mM NaCl, 0.5% Triton X-100, 1 mM EDTA, 1 mM EGTA, 10 mM NaF, 2.5 mM NaVO4, cOmplete protease inhibitor Cocktail (Roche), 1X Phosphatase Inhibitor Cocktail 2 (Sigma-P57726), 1X Phosphatase Inhibitor Cocktail 3 (Sigma-P0044)). Samples were sonicated, clarified by centrifugation, filtered and stored at −80°C. RNA and genomic DNA were also extracted from parental and resistant cell lines by using the AllPrep® DNA/RNA Mini Kit (Qiagen). RNA and DNA quality was verified using Agilent RNA 6000 Nano Kit and Agilent High Sensitivity DNA Kit (Agilent Technology). DNA quantity was assessed by Qubit® dsDNA BR Assay Kit (Thermo Fisher Scientific). Biological duplicates were analyzed for each sample.

Use of Multiplexed Inhibitor Beads (MIBs) to Analyze the Kinomes of Drug-sensitive and -resistant *Nf1* Cells

Multiplexed Inhibitor Beads (MIB) chromatography and quantitative mass spectrometry (MS) methodology was performed as described previously (43) to examine the kinomes of PD901 or RAD001 resistant *Nf1* cell lines and matched parentals. The LFQ (label free quantification) intensity is the normalized abundance across all runs and relative to all identified proteins (typically in the 10e5 to 10e9 range). 194 kinases divided in 11 kinase families were selected by filtering "Razor + unique peptides" number which was set ≥ 2. Log2LFQs were calculated and used for further analyses and comparisons. Averages of Log2LFQ duplicates were calculated. Log2LFQ averages of parental cell lines (989 and 881) were subtracted from the Log2LFQ averages of drug-resistant or drug-sensitive counterparts (989 PD_R, 989 RAD_R, 881 PD_R, 989 + PD, 989 + RAD, 881 + PD, 881 + RAD). Heat maps were created using Morpheus and the color scale represents Z-score. Cytoscape software integrated with Genemania was used to visualize large scale integration of molecular interaction network data. Kinases lists were imputed in Genemania to determine physical interactions that were then integrated in the Cytoscape for visualizing kinase-kinase network. Log2LFQ differences >1 or <−1 were included in visualizing the protein interactions.

Whole Transcriptome—Total RNA (1 microgram) was used as input for Illumina's TruSeq stranded mRNA library preparation protocol. The libraries were made according to the manufacturer's instructions. Library quality and quantity were assessed using the

Agilent 2200 TapeStation instrument prior to sequencing. Paired-end 75 bp reads were generated using Illumina NextSeq500 with the high output 150-cycle flowcell. For pathway enrichment analysis, we computed the up/down regulated genes in RAD_R vs P and PD_R vs P in the 989 PD_R and 989 RAD_R cell lines. Specifically, consistently differentially expressed genes in each cell line were analyzed in a generalized linear model to compute the differential gene expression test ($p<0.001$ as a significant cutoff).

Bioinformatics Analysis—RAW sequencing data (fastq files) were mapped to the mouse mm10 genome by using STAR pipeline (44). On average, 65.4% reads were uniquely mapped to the exon regions and were used to compute the counts mapped to each gene. DESeq2 was applied identify differentially expressed genes among the conditions, with FDR<0.05 and log fold change >1.0 or <−1.0, as the significance cutoff. MDS plots and heatmaps were plotted using the log(RPKM+1) normalized gene expression levels. All the sample-wise clustering analysis utilized the hierarchical clustering method (*hclust* function) by R with the default setting.

Whole exome sequencing

Library Preparation and Sequencing and informatics—Whole Exome Sequencing as performed on two biological replicates of each cell line. Whole Exome Sequence Analysis Genomic DNA was extracted from cells using standard, previously described methods (45). All sequence data including read alignment (to mm10 build) quality and performance metrics post-processing, somatic mutation detection; and variant annotation were performed as previously described (46) using the mm10 build of the mouse genome.

RESULTS

Nf1 mutant tumor cell lines demonstrate variable basal RAS signaling

The *NF1* gene product is the RAS-GTPase activating protein neurofibromin, which negatively regulates RAS. Loss of neurofibromin leads to RAS activation, commonly involving two main signaling pathways downstream of RAS, RAF/MEK/ERK and PI3K/AKT/mTOR. We compared RAS signaling profiles in 12 *Nf1* null mouse tumor cell lines derived from radiation-induced tumors arising in *Nf1* heterozygous mice (14, 16). Tumor histologies included mammary carcinomas, squamous cell carcinomas, and soft tissue sarcomas (13, 14). These malignancies were previously analyzed for genetic variants, indicating that these malignancies demonstrate loss of wildtype *Nf1* and *Trp53* in cis via loss of a large segment of chromosome 11 (13). While these tumor cell lines share genetic loss of *Nf1* as an initiating feature, western blotting analysis of PI3K-mTOR and RAF-MEK revealed differences in basal RAS signaling among our cell lines when grown in the presence of serum, as evidenced by variable phosphorylation of RAS effectors (Fig. 1A).

We then assessed Ras activity in the context of serum starvation followed by serum stimulation. After 24 hours of serum starvation, cells were stimulated for 0, 5, 30 and 60 minutes with medium supplied with 10% FBS, then protein lysates were collected. All tumor cell lines demonstrated increased RAS-GTP at 5 minutes post-stimulation with variable kinetics of attenuation (Fig. 1B and S1A). In contrast to the basal Ras pathway

signaling, stimulation after serum starvation was uniformly associated with sustained activation of RAS-GTP and downstream effectors such as phosphorylated AKT (S473), S6 (Ser235/236) and p44/42 MAPK (ERK1/2) (Thr202/Tyr204), although even a subset of these (881, 917, 9223 and 989) demonstrated relatively more activation of RAS-GTP and downstream effectors. (Fig. 1B and S1A). These comparisons between signaling under either basal or starvation-stimulation conditions reveal that genetic *Nf1*-deficient tumor cell lines share intact core Ras pathway activation when acutely stimulated but under basal growth conditions diverge to non-uniform Ras pathway activation.

Wildtype *RAS* in *Nf1* null tumors

The variability in RAS pathway activation led us to ask whether these *Nf1* mutant tumors harbored mutant RAS, the presence of which could produce constitutive activation and amplify downstream signaling above that achieved with wildtype RAS. *NF1* and *RAS* are uncommonly co-mutated in cancer, but *NF1* and other RASopathy genes have been found to be co-mutated in melanomas (6). To identify activating Ras mutations we sequenced exons 2 and 3 of *Kras*, *Nras* and *HRas* in our 12 *Nf1* mutant mouse tumor cell lines.

Ras mutations infrequently co-occurred with *Nf1* loss in our mouse model of *Nf1*-driven tumorigenesis. Of the twelve lines sequenced, one cell line (cell line 169) harbored a somatic mutation in codon 12 of *Hras* (Fig. S2A–B). This point mutation involves a recognized hotspot residue that is implicated in binding nucleotide phosphates (17–19), substituting a guanine for an adenine (GGA>GAA), replacing a glycine for a negatively charged glutamic acid (G12E) in the protein. Notably Ras-GTP activation and downstream signaling after serum stimulation is similar between the cell line 169 and other *Nf1* mutant cell lines with wildtype *Ras* (Fig. 1B), suggesting that this Ras mutation fails to amplify Ras signaling beyond that achieved by *Nf1* loss alone. These data indicate that acquired *Ras* mutations are uncommon in our genetic model of *Nf1*-driven tumorgenesis and thus do not explain Ras signaling heterogeneity in this system.

Transcriptome and functional kinome heterogeneity in parental *Nf1* null tumors

The apparent heterogeneity in Ras signaling among the panel of cell lines indicates that *Nf1* loss does not produce a common shared Ras signaling signature and suggests underlying heterogeneity in kinome function. Rather than focusing the analysis on cell lines functioning at extremes of signaling, we focused analysis on a subset of cells to investigate genetic, transcriptomic and kinome differences, these being 881 and 989 lines because they are both mouse sarcoma cell lines that share similar kinetics of Ras signaling after starvation followed by stimulation (Fig. 1B), showing peaking of pAKT and pERK at 5 minutes post-stimulation.

Transcriptome and kinome profiling of the 989 and 881 lines demonstrated that although these lines share *Nf1* loss and similar basal and stimulated PI3K/AKT and MAPK pathway activation, kinome-wide differences distinguish these lines (Fig. 1C). The five kinases in each cell line exhibiting the greatest MIB binding (Fig. S1B) were also transcriptionally upregulated (Fig. 1D). Cytoscape software integrated with Genemania was used to visualize protein interaction networks constituted by the kinomes of the 881 and 989 cell lines (Fig.

S3A–S3B). Network analysis revealed that Aurora Kinase (AURKA) was among the kinases demonstrating increased MIB binding common between these two cell lines (Fig. S3A).

Aurora Kinases (AURKs) are involved in mitotic control and inhibitors of AURKs have been shown to have therapeutic potential against cancers (20). To test whether AURKA identified by kinome analysis is functionally relevant to growth in our tumor cell lines, we assessed pharmacologic inhibition of AURKA in the parental cell lines 881 and 989. We assessed the AURKA inhibitor MLN827, and for comparative purposes the AURKB inhibitor AZD1152 and the pan-AURK inhibitor VX680, each decreasing phosphorylation levels of their respective targets (Fig. S3C and S3D). AURK inhibition reduced growth of both the 989 and 881 cell lines, although AURKA inhibition with MLN827 produced the greatest negative effect on cell viability, validating the identification of AURKA as a functionally relevant kinase that supports growth by both 989 and 881 *Nf1* mutant cell lines.

Derivation of MEKi- or mTORi-resistant *Nf1* mutant tumor cell lines

The development of drug resistance by tumors is an important clinical problem that can involve different mechanisms, such as new mutations in the drug target, activation of redundant biological feedback loops or overexpression of proteins that compensate for the loss of the drug target. Notably the 989 and 881 cell lines share similar phosphorylation response profiles to PD901, CI1040 (an ATP non-competitive MEK inhibitor), PP242 (an ATP-competitive mTOR inhibitor), PIK75 (PI3K inhibitor), RAD001, and BEZ235 (dual PI3K/mTOR inhibitor) (Fig. S4) and we sought to determine whether the similar biochemical responses present in these two lines would extend to the drug-resistant setting.

The best studied therapeutic approaches in NF1 mutant tumors include pharmacologic inhibition of MEK and mTOR (10). To model the emergence of resistance to chronic MEKi or mTORi, we cultured parental *Nf1* 989 and 881 cell lines in the MEK inhibitor (MEKi) PD0325901 (PD901, an ATP non-competitive MEK inhibitor) or the mTOR inhibitor (mTORi) RAD001 (a rapalog mTOR inhibitor). Drug-resistant derivatives were established by exposing parental 989 and 881 lines to increasing concentrations (from 25 nM up to 500 nM) of either PD901 or RAD001 continuously in the media. Resistant cell lines were pooled cells that were continuously maintained in medium supplemented with inhibitor. Two sets of resistant cell lines were established from each chronic drug exposure, cultured in either 100 nM (PD_R1 and RAD_R1) or 500 nM (PD_R and RAD_R). 989 and 881 resistant derivatives are referred to as 989 PD_R, 881 PD_R, 989 RAD_R, and 881 RAD_R (MEKi and mTORi resistant, respectively). Culturing cells in 500 nM PD901 produced acquired drug-resistance in both lines (Fig. 2A and S5A). In contrast, extended chronic exposure to escalating concentrations of RAD001 led to the development of a relative resistance to RAD001 compared to the parental line, rather than the complete resistance developed after PD901 exposure.

The apparent similarities in Ras signaling between the parental 989 and 881 were lost in the setting of acquired drug resistance. The biochemical changes in Ras signaling varied between cell lines; compared to matched parental cells, levels of pAKT and pS6 markedly increased in 989 PD_R cells compared to parental, whereas 881 PD_R cells lacked this response (Fig. 2B and S5B). While basal pAKT and pERK levels decreased in 989 RAD_R

cells compared to parental, the 881 RAD_R cells demonstrated an increase in these effectors compared to parental 881 cells (Fig. 2B and S5B).

To compare Ras activation in response to stimulation by serum, cells were serum starved for 24 hours then stimulated for 0, 5, 30 and 60 min with serum containing media after which protein lysates were collected. RAS-GTP levels were assessed by GTPase pull-down. Acquired resistance to MAPK or mTOR inhibition was associated with altered basal Ras pathway activation as well as in response to inhibitor exposure (Fig. 2E, Fig. S5). Notably, for both cell lines phosphorylated S6 and ERK, readouts of biochemical response to RAD and PD901, respectively, remain suppressed in drug-resistant derivatives, indicating that re-activation of these pathways does not occur.

Combinatorial kinome inhibition is a strategy employed to improve treatment efficacy, and we assessed the sensitivity of PD_R cells to RAD001 and RAD_R cells to PD901. Both 989 PD_R and 881 PD_R cell lines show sensitivity to RAD treatment alone (Fig. 2D,E and S5C). PD901 decreased cell viability in both the 989 RAD_R and the 881 RAD_R cell lines (Figs. 2D and S5D). Finally, combined PD901 and RAD001 produced the greatest suppression of cell viability in both sets of drug-resistant derivatives, pointing to the combined importance of each of these pathways in promoting proliferation (Fig. 2E and S5C).

Acquired drug resistance confers resistance to other shared pathway inhibitors

The mechanisms responsible for acquired drug resistance may impact processes mediating sensitivity to other drugs, and this can be a point of differentiating between cell lines and types of acquired drug resistance. The issue of cross-resistance, whereby resistance to one kinase inhibitor confers resistance to other inhibitors, is a clinically significant issue and challenging to predict. We analyzed drug resistant derivatives for the acquisition of resistance to other kinase inhibitors. AURKA is a functionally relevant kinase that supports growth by both parental 989 and 881 *Nf1* mutant cell lines (Fig. S3); we assessed whether acquired resistance to either MEKi or mTORi also conferred resistance to AURKA inhibition. Both RAD_R cell lines and the 881 PD_R cell line retained sensitivity to all three Aurora inhibitors (with AZD1152 producing the weakest response), demonstrating decreased cell growth and phosphorylation of AURKA, AURKB and H3 (Fig. S6A and S6B). The 989 PD_R cells were the exception among the drug resistant derivatives, demonstrating resistance to Aurora inhibitor AZD1152 alone as well as when combined with PD901 (Fig. S6A). The 989 PD_R tumor cells serve as an example of how tumor cells that acquire resistance to one inhibitor (MEKi) can acquire resistance to inhibitors of other molecular classes (AURK), although given that this did not also occur in the 881 PD_R cells we can surmise that this cross-resistance is cell-specific rather than a generalized feature of resistance to MEKi.

Drug resistant derivatives were also challenged with alternative MEK and mTOR inhibitors (MEK162, Trametinib, BEZ235 and rapamycin) already approved for clinical use or tested in different clinical trials. Parental and PD-resistant 881 cells were unaffected by the MEK162 (Fig. S7), however, the RAD-resistant 881 RAD_R acquired sensitivity to MEK162 (Fig S7). This acquired sensitivity was not similarly observed in the 989 lines

(parental and drug resistant derivatives), all of which, similar to the parental 881 line, remained resistant to MEK162. BEZ235, a dual PI3K and mTOR inhibitor markedly suppressed the growth of all drug resistant cell lines (Fig. S7) (21), indicating that *Nf1* mutant tumor cells acquiring resistance to either MEKi or mTORi continue to be functionally dependent on PI3K.

We compared the transcriptomes of 989 cells treated with either acute or chronic MEKi and mTORi (989 PD_R and 989 RAD_R) (Fig. 3A) to parental 989 cells using unsupervised hierarchical clustering (Fig. 3B). This analysis indicated that parental and acutely-treated parental cells (989+PD9901 and 989+RAD001) retained transcriptomic similarity as a group, while drug-resistant cell lines clustered separately from parental treatment groups and controls (Fig. 3B and S8A). Overall, acutely treated cells (with either PD901 or RAD001) demonstrated significantly fewer differentially expressed genes as compared to 989 PD_R and 989 RAD_R cell lines (Fig. 3C).

Given the significant changes in expression associated with acquired drug resistance, we performed pathway enrichment analysis to identify preferentially affected biological processes. We first computed the pathways enriched by differentially expressed genes (DEG) ($p<0.01$). We then analyzed DEGs in a generalized linear model ($p<0.001$ as a significant cutoff) and found a very significant overlap between the DEG lists of RAD_R vs P and PD_R vs P, $p<1e-16$ for both up and downregulated genes in the two resistant lines (Supplementary Table 3). This analysis identified pathway enrichment shared between the drug resistant cell lines; significantly increased gene expression in extracellular matrix organization pathway occurred in both RAD and PD-resistant cell lines. Genes significantly downregulated in both resistant cell lines commonly functioned in pathways modulating metabolism of non-coding RNA and mRNA processing.

To determine how acute versus chronic drug exposure differ in effects on the kinome, we used multiplexed inhibitor beads coupled with mass spectrometry (MIB/MS) to quantitatively measure dynamic changes in kinase activity. For this analysis, we compared parental 989 tumor cells that were acutely treated with either PD901 or RAD001 (for 24 hours) and drug-resistant 989 tumor cells that were continuously grown in either of these drugs (989 PD_R or 989 RAD_R). Figure 3D shows these four experimental groups that are each compared to control untreated parental cells: the drug resistant cell lines 989 PD-R, 989 RAD-R, and the parental cell lines treated with either drug acutely. The heat map depicts the subtraction of the average kinase Log2LFQ (194 total) of two biological replicates of parental cell lines from the average Log2LFQs of two biological replicates of resistant or acutely-treated cells. Thus, untreated parental controls were analyzed in parallel with drug-treated cells and the data is displayed as the difference from untreated parental controls.

Kinome analysis distinguishes drug-resistant cells from acutely treated cells (Fig. 3D). One hundred and ninety four kinases were assayed in resistant and acutely treated 989 cells and compared to untreated parental 989 cells; the differences in MIB binding between drug-treated cells and parental controls are visualized as a heatmap in which kinases are organized into 11 kinase families (Fig. 3D). Strikingly, the kinome profiles of the drug resistant 989

cells segregated from acutely treated cells, irrespective of the drug target, supporting the concept that *Nf1* mutant tumors undergo broader remodeling of kinome activity in response to targeted kinase inhibition.

Integrated kinome and RNA-Seq analyses of PD901- and RAD001-resistant *Nf1* cell lines (compared to parental) indicate that changes in the functional kinome generally correlate with mRNA expression changes (Fig. 4A). Kinome data were organized into molecular interaction networks for PD_R and RAD_R cell lines (S8B-G).

Common, shared changes in specific kinases were identified in drug resistant cells (Fig. 4B–E), with the MIB binding of some kinases correlating with changes in transcription (Fig. 4A). Shared kinases with increased MIB binding were diverse, and apparently not functionally linked to each other or to MAPK and PIK3 signaling pathways, thus representing potentially new mechanisms of therapeutic relevance. Shared kinases included those involved in metabolism, such as PFKM (Phosphofructokinase, Muscle) (22), as well as CDK18 (Cyclin Dependent Kinase 18) (23) and CHEK1 (Checkpoint Kinase 1) (24), which are involved in DNA repair (Fig. 4B).

Interestingly, drug resistance was associated with reduced MIB binding of three functional classes of kinases (Fig. 4C). Kinases involved in metabolism demonstrated significantly reduced binding; these included HK2 (Hexokinase 2), which catalyzes the first essential step of glucose metabolism, the conversion of the substrate glucose into glucose-6-phosphate (25) and the mitochondrial enzyme PCK2 (Phosphoenolpyruvate Carboxykinase 2), which catalyzes the conversion of oxaloacetate to phosphoenolpyruvate in the presence of guanosine triphosphate (GTP) (26, 27). Growth factor receptors EGFR (Epidermal Growth Factor Receptor) and PDGFRA (Platelet Derived Growth Factor Receptor Alpha) demonstrated reduced MIB binding in the setting of drug resistance (Fig. 4C). Three protein kinases involved in the PIP2 pathway were downregulated in both 989 PD_R and 989 RAD_R cell lines, these being two PRKC isoforms, PRKCA (Protein Kinase C Alpha) and PRKCD (Protein Kinase C Delta), and one of their downstream effectors PRKD2 (Protein Kinase D2) (Fig. 4C). The calcium-activated PRKCA kinase can promote cell growth by phosphorylating and activating RAF1, which mediates the activation of the MAPK/ERK signaling cascade (28).

Notably, few kinases were commonly altered in MEKi resistant cell lines (989 PD_R and 881 PD_R) (Fig. 4D–E). EPHB2 exhibited increased MIB binding in both PD901 resistant lines (989 PD_R and 881 PD_R, Fig. 4D) and also in the 989 RAD_R line, making it the only kinase demonstrating increased MIB binding in all three cell lines analyzed. EPHB2 (Ephrin type-B receptor 2) is a member of the largest family of receptor tyrosine kinases in the mammalian genome and demonstrated increased MIB binding in both. EPHB2 is capable of activating MAPK pathway inhibition and has been described to modulate multiple cancer cell behaviors, such as invasion, dedifferentiation and metastasis (29) (30). Consistent with pharmacologic inhibition, reduced MIB binding was observed for MAP2K1/MEK1 in cells chronically treated with MEKi (Fig. 4E).

Private and shared somatic variants distinguish drug resistant derivatives from parental cells

The kinome profiles of resistant phenotypes revealed a limited number of targetable nodes however the drug-resistance can also be driven by the genetic events such as acquired somatic variants. To investigate this we performed whole exome sequencing analysis of the parental 989 cell line, its matched drug-resistant derivatives and germline (tail) control to identify somatic single nucleotide variants and compare the mutational profile amongst these lines. Somatic single nucleotide variants (SNVs) were quantified in each cell line.

Acquired drug resistance was associated with unique somatic variants in the exomes of resistant lines that were not present in the parental lines. Both 989 PD_R and 989 RAD_R resistant cell lines harbored more somatic SNVs than the parental line from which they were derived (Fig. 5A). The degree of genetic similarity between parental and drug-resistant derivatives can be inferred from the percentage of somatic variants that are shared or private; the numbers of shared and private somatic SNVs amongst 989, 989 PD_R and 989 RAD_R are shown in Fig. 5A/B. One hundred and thirty somatic SNVs were shared among all three cell lines. 989 PD_R and 989 RAD_R cell lines shared 39 SNVs, suggesting that these SNVs are not drug-specific. Expressing the private and shared somatic SNVs as percentages of each cell line's total somatic SNVs (Fig. 5B), we find that private mutations in 989 PD_R and 989 RAD_R comprised 54.33% and 33.95% of the total somatic SNVs, respectively.

These analyses indicate that acquired drug resistance is associated with increased genetic diversity, evidenced by minor retention of parental somatic SNVs resulting in fewer than 5% of somatic SNVs in either drug-resistant line being shared exclusively with the parental line. Interestingly, a greater proportion of somatic SNVs was shared only by the drug-resistant lines, suggesting possibly common resistance variants (Fig. 5A–B).

Molecular pathways involved with somatic mutations in drug resistant cell lines included pathways regulating release of intracellular calcium and PKC activation. *Plcd3* (1-phosphatidylinositol 4,5-bisphosphate phosphodiesterase delta-3) hydrolyzes the phosphatidylinositol 4,5-bisphosphate (PIP2) to generate the second messenger molecules diacylglycerol and inositol 1,4,5-trisphosphate (IP3) (31), and was mutated in 989 PD_R cell line. *Ptprq* (Phosphatidylinositol phosphatase), which regulates the phosphorylation state of AKT1 by suppressing the phosphatidylinositol 3,4,5-trisphosphate (PIP3) level (32), was also mutated in 989 PD_R cell line. *Dgkq* (Diacylglycerol kinase theta), which phosphorylates diacylglycerol to generate phosphatidic acid (PA) (33), was mutated in both 989 resistant cell lines (Supplementary Table 1).

The 989 PD_R and 989 RAD_R cell lines shared a mutation in the gene *Nuclear factor related to kappa-B-binding protein* (*Nfrkb)* (Fig. 5C). NFRKB is a member of the chromatin remodeling INO80 complex and binds to the DNA consensus sequence 5'-GGGGAATCTCC-3' (34). WES and RNA-Seq each identified the same somatic mutation in the *Nfrkb* gene in both 989 resistant cell lines (Fig. 5C). The NFRKB protein sequence is highly conserved in multiple species (35); the point mutation acquired by drug-resistant 989 cell lines substitutes a cytosine for a guanine (CCG>CGG) in position 223, replacing a proline for an alanine (P75A). Due to the large size of the protein, the full-length NFRKB

structure has not yet been determined, however mutations throughout the NFRKB protein have been identified in human cancers (COSMIC database, https://cancer.sanger.ac.uk/cosmic/) and the overall distribution of somatic SNVs is suggestive of NFRKB functioning as a tumor suppressor.

Stability of PD901-resistance

Managing drug-resistant cancers is a practical challenge and effective strategies are likely defined by the mechanisms by which drug-resistance develops and whether these mechanisms are reversible. Drug-resistant tumors can develop an addiction-like state that renders them sensitive to drug withdrawal (36), a characteristic that may support discontinuation of a drug. We sought to test whether drug-resistant *Nf1*-null tumor lines demonstrate drug addiction evidenced by sensitivity to drug withdrawal. Drug-resistant 989 and 881 lines were grown in drug-free media (named washout, “WO”) for one week (989 PD_R WO, 989 RAD_R WO, 881 PD_R WO, 881 RAD_R WO) then cell viability was compared to parental and drug-resistant lines (Fig. 6A–B).

After drug washout both 989 RAD_R WO and 881 RAD_R WO demonstrated significantly reduced growth as compared to the lines from which they were derived, 989 RAD_R and 881 RAD_R (Fig. 6B). In contrast, 989 PD_R WO and 881 PD_R WO maintained growth and retained their resistance to PD901 (Fig. 6A). Phosphorylated ERK1/2 in 989 PD_R WO cells after drug washout failed to recover to parental levels (Fig. 6C) suggesting that the development of resistance to MEKi is associated with stable impaired MAPK signaling. Notably, withdrawing drug from 989 RAD_R cells (989 RAD_R WO) resulted in impaired growth compared to parental control cells despite the recovery of mTOR signaling, as evidenced by phospho S6 and phospho Akt (Fig. 6D). Re-exposure of both 989 RAD_R WO and 881 RAD_R WO cells to RAD was associated with complete loss of phosphorylated S6, recapitulating the original RAD-resistant 989 and 881 lines. These data contrast chronic MEKi with chronic mTORi with respect to drug addiction and reconstituting inhibition observed in drug-naïve cells; chronic mTORi was associated with drug dependence in both *Nf1* mutant cell lines and reduced growth upon drug withdrawal, while this response was absent in PD-resistant *Nf1* mutant cell lines tested in parallel.

Our analysis of acquired drug resistant cell lines demonstrated that drug exposure is associated with extensive transcriptomic changes that distinguish drug resistant cells from parental cells (Figure 3C). To investigate the stability of these transcriptomic alterations we then asked whether drug withdrawal might reveal stable versus reversible transcriptomic changes after chronic drug exposure. We compared the transcriptomes of WO cells to the drug resistant cells from which they were derived and the parental cells from which all drug-exposed cells were derived. Unsupervised hierarchical clustering analysis distinguishes 989 PD_R WO and 881 PD_R WO from the 989 PD_R and 881 PD_R lines (Fig. 6E and S8C), suggesting that drug withdrawal itself triggers a transcriptomic response. Notably, hierarchical clustering analysis restricted to only kinome transcripts (Fig. 6E) differentiate 989 PD_R and 989 PD_R WO from drug-resistant and parental cells, suggesting that the kinome robustly reflects cellular adaptations in response to MEKi. In neither cell line does drug washout restore the kinome to the parental state (Fig. 6E), providing evidence that

kinome-wide consequences of MEKi or mTORi are relatively irreversible. Collectively these findings indicate separate fates associated with prolonged drug exposure, with MEKi being associated with irreversible drug resistance while mTORi failed to produce complete and durable drug resistance (Fig. 6F).

DISCUSSION

Tumors harboring *NF1* mutations are classified as a subtype of RASopathies. Although *Nf1* loss is the shared genetic alteration leading to neoplastic progression in NF1, our data indicate that loss of heterozygosity of *Nf1* as an initial genetic event does not confer a common functional signature. We interrogated a unique set of murine *Nf1* mutant tumors to assess the biochemical and functional spectrum in this genetic class, and in so doing identified basal Ras pathway activation and variable responses to kinase inhibition. These data demonstrate basal heterogeneity in Ras signaling in the context of dysregulated but largely wildtype Ras signaling. Furthermore, in the absence of a strong driver such as oncogenic Ras, *Nf1*-null tumors, in which Ras pathway activation is heterogeneous, may be uniquely positioned to utilize diverse mechanisms to circumvent drug therapy.

Employing multiple approaches to investigate the genetic and functional similarities among *Nf1* mutant tumors we uncovered shared vulnerabilities; for example kinome profiling of parental *Nf1* null tumor lines identified overlap with respect to kinase affinity (Fig. S3). Among the activated kinases common to the *Nf1* null cell lines was Aurora Kinase A (AURKA). Interestingly, AURKA is not a canonical Ras pathway effector, but represented a common therapeutic target, as the AURKA inhibitor MLN8237 decreased phospho-AURKA levels and reduced cell growth. Importantly, AURKA is not known to have a prominent function in *NF1* mutant cancers and thus its identification represents a novel opportunity. AURKA inhibition has been employed to overcome drug resistance in several cancers (37, 38), and targeting AURKA in *Nf1* null neoplasms might similarly serve as a strategy to prevent or delay drug resistance.

Our study examines the biochemical consequences of chronic mTOR inhibition and demonstrates that the signaling consequences of prolonged inhibition differ from the acute effects. RAD001 inhibits mTORC1, which can trigger a negative feedback loop resulting in AKT S473 phosphorylation by mTORC2 (39). However, prolonged rapamycin treatment (over hours to days) has been described to inhibit mTORC2 assembly and subsequently decrease phosphorylation of Akt S472 (40). We found that *Nf1* mutant tumor cells chronically exposed to RAD001 demonstrate downregulated phosphorylation of both ERK and AKT compared to their matched parental lines (Fig 2C). Similarly, increasing concentrations of rapamycin treatment (100 nM and 1000 nM) for 24 hours in cancer cells produces a dose-dependent reduction in phospho-ERK (41) in an mTORC2-dependent manner. The reduced phospho-ERK observed in RAD001-resistant 989 cells likely reflects the same phenomenon, similar to AKT.

Tumors evolve and can develop complex genomic alterations in response to therapy (42). These post-therapy alterations can have important therapeutic implications, however neither post-treatment nor drug-resistant *NF1* mutant tumors have been characterized to date.

To study the consequences of inhibitor-mediated selective pressure leading to a therapy-resistant tumor cell population, we modeled the emergence of drug-resistant *Nf1* tumors in response to chronic MEKi or mTORi. This approach enabled systematic comparisons between experimentally-derived drug-resistant cells and matched original parental lines. These analyses revealed functional remodeling of the kinome, as evidenced by significant changes in MIB binding and transcript abundance developing in the setting of both MEKi and mTORi. Importantly, comparing MIB binding between resistant cell lines revealed few kinases commonly increased or decreased between pairs of drug resistant cells, but the greatest overlap or shared kinases between 989 PD_R and 989 RAD_R (Figure 4B/C).

MEKi and mTORi-resistant tumors were genetically distinct; somatic SNVs were predominantly unique acquired mutations, with minor representation of parental SNVs. Also notable was the absence of *RAS* mutations in drug-resistant cell lines, indicating that *Nf1*-driven tumorigenesis and responses to therapy occur in the context of wildtype Ras. The propensity of drug-resistant tumors to acquire a significant proportion of private mutations, thereby becoming ‘less related’ to the original parental tumor, resists attempts to neatly classify drug-resistant disease on a genetic basis. Given this challenge and suggested heterogeneity in genetic alterations post-therapy, our findings highlight the need for studies directed to this issue. Further analyses of greater numbers and types of post-treatment tumors, experimental and clinical, will be needed to elucidate the most common or dominant mutational motifs.

Drug resistance can be associated with addiction, whereby drug withdrawal results in loss of essential growth signals and subsequent tumor regression. Interestingly, RAD resistant cell lines demonstrated evidence of drug addiction whereas PD resistant cells did not. Upon drug withdrawal, RAD-resistant lines reverted to their parental mTOR signaling and re-exposure to RAD re-constituted inhibition of mTOR. In contrast, following drug cessation, PD_R WO cell lines maintained similar functional and biochemical mechanisms to the PD_R cells. Our data show that drug addiction develops in a drug-specific manner, a finding that supports therapeutic strategies tailored to specific drug resistance, for example a drug holiday for mTORi resistant cells and mTORi for MEKi resistant cells.

In summary, tumorigenesis initiated by *Nf1* loss is mediated in the context of wildtype Ras and produces biochemically heterogeneous cancers. This diversity is apparent in the basal signaling, response to therapeutics and subsequent acquired drug resistance. *Nf1* mutant tumors treated with MEKi and mTORi, the two most commonly utilized therapeutic approaches against hyperactive Ras signaling in NF1 neoplasms, acquire genetic and transcriptomic alterations distinguishing them from parental tumors. The reversibility of these changes is defined in a drug-dependent manner and therapeutic strategies in the post-treatment context must be informed by data specific to the clinical scenario.

Supplementary Material

Refer to Web version on PubMed Central for supplementary material.

ACKNOWLEDGEMENTS

We thank Benjamin Braun and his lab for helpful discussions. JLN was supported by a gift from the Hagar Family Foundation and the Department of Defense (W81XWH1810287). JLN, KS, WC, GLJ, SA, and CZ were supported by U54 CA196519 (NIH/NCI).

REFERENCES

1. Buck E, Eyzaguirre A, Rosenfeld-Franklin M, Thomson S, Mulvihill M, Barr S, Brown E, O'Connor M, Yao Y, Pachter J, Miglarese M, Epstein D, Iwata KK, Haley JD, Gibson NW, Ji QS. Feedback mechanisms promote cooperativity for small molecule inhibitors of epidermal and insulin-like growth factor receptors. Cancer Res. 2008;68(20):8322–32. doi: 10.1158/0008-5472.CAN-07-6720. [PubMed: 18922904]
2. Gioeli D, Wunderlich W, Sebolt-Leopold J, Bekiranov S, Wulfkuhle JD, Petricoin EF 3rd, Conaway M, Weber MJ. Compensatory pathways induced by MEK inhibition are effective drug targets for combination therapy against castration-resistant prostate cancer. Mol Cancer Ther. 2011;10(9):1581–90. doi: 10.1158/1535-7163.MCT-10-1033. [PubMed: 21712477]
3. Chen CH, Hsia TC, Yeh MH, Chen TW, Chen YJ, Chen JT, Wei YL, Tu CY, Huang WC. MEK inhibitors induce Akt activation and drug resistance by suppressing negative feedback ERK-mediated HER2 phosphorylation at Thr701. Mol Oncol. 2017;11(9):1273–87. doi: 10.1002/1878-0261.12102. [PubMed: 28632938]
4. Stewart A, Coker EA, Polsterl S, Georgiou A, Minchom AR, Carreira S, Cunningham D, O'Brien ME, Raynaud FI, de Bono JS, Al-Lazikani B, Banerji U. Differences in Signaling Patterns on PI3K Inhibition Reveal Context Specificity in KRAS-Mutant Cancers. Mol Cancer Ther. 2019;18(8):1396–404. doi: 10.1158/1535-7163.MCT-18-0727. [PubMed: 31262731]
5. Ratner N, Miller SJ. A RASopathy gene commonly mutated in cancer: the neurofibromatosis type 1 tumour suppressor. Nat Rev Cancer. 2015;15(5):290–301. doi: 10.1038/nrc3911. [PubMed: 25877329]
6. Philpott C, Tovell H, Frayling IM, Cooper DN, Upadhyaya M. The NF1 somatic mutational landscape in sporadic human cancers. Human genomics. 2017;11(1):13. doi: 10.1186/s40246-017-0109-3. [PubMed: 28637487]
7. Ambrosini G, Cheema HS, Seelman S, Teed A, Sambol EB, Singer S, Schwartz GK. Sorafenib inhibits growth and mitogen-activated protein kinase signaling in malignant peripheral nerve sheath cells. Mol Cancer Ther. 2008;7(4):890–6. doi: 10.1158/1535-7163.MCT-07-0518. [PubMed: 18413802]
8. Jessen WJ, Miller SJ, Jousma E, Wu J, Rizvi TA, Brundage ME, Eaves D, Widemann B, Kim MO, Dombi E, Sabo J, Hardiman Dudley A, Niwa-Kawakita M, Page GP, Giovannini M, Aronow BJ, Cripe TP, Ratner N. MEK inhibition exhibits efficacy in human and mouse neurofibromatosis tumors. J Clin Invest. 2013;123(1):340–7. Epub 2012/12/12. doi: 60578 [pii] 10.1172/JCI60578. [PubMed: 23221341]
9. Staser K, Park SJ, Rhodes SD, Zeng Y, He YZ, Shew MA, Gehlhausen JR, Cerabona D, Menon K, Chen S, Sun Z, Yuan J, Ingram DA, Nalepa G, Yang FC, Clapp DW. Normal hematopoiesis and neurofibromin-deficient myeloproliferative disease require Erk. J Clin Invest. 2013;123(1):329–34. Epub 2012/12/12. doi: 66167 [pii] 10.1172/JCI66167. [PubMed: 23221339]
10. Gross AM, Frone M, Gripp KW, Gelb BD, Schoyer L, Schill L, Stronach B, Biesecker LG, Esposito D, Hernandez ER, Legius E, Loh ML, Martin S, Morrison DK, Rauen KA, Wolters PL, Zand D, McCormick F, Savage SA, Stewart DR, Widemann BC, Yohe ME. Advancing RAS/RASopathy therapies: An NCI-sponsored intramural and extramural collaboration for the study of RASopathies. Am J Med Genet A. 2020;182(4):866–76. doi: 10.1002/ajmg.a.61485. [PubMed: 31913576]
11. Malone CF, Fromm JA, Maertens O, DeRaedt T, Ingraham R, Cichowski K. Defining key signaling nodes and therapeutic biomarkers in NF1-mutant cancers. Cancer discovery. 2014;4(9):1062–73. doi: 10.1158/2159-8290.CD-14-0159. [PubMed: 24913553]
12. Robertson KA, Nalepa G, Yang FC, Bowers DC, Ho CY, Hutchins GD, Croop JM, Vik TA, Denne SC, Parada LF, Hingtgen CM, Walsh LE, Yu M, Pradhan KR, Edwards-Brown MK, Cohen MD,

Fletcher JW, Travers JB, Staser KW, Lee MW, Sherman MR, Davis CJ, Miller LC, Ingram DA, Clapp DW. Imatinib mesylate for plexiform neurofibromas in patients with neurofibromatosis type 1: a phase 2 trial. Lancet Oncol. 2012;13(12):1218–24. doi: 10.1016/S1470-2045(12)70414-X. [PubMed: 23099009]

13. Nakamura JL, Phong C, Pinarbasi E, Kogan SC, Vandenberg S, Horvai AE, Faddegon BA, Fiedler D, Shokat K, Houseman BT, Chao R, Pieper RO, Shannon K. Dose-dependent effects of focal fractionated irradiation on secondary malignant neoplasms in Nf1 mutant mice. Cancer Res. 2011;71(1):106–15. Epub 2011/01/05. doi: 71/1/106 [pii] 10.1158/0008-5472.CAN-10-2732. [PubMed: 21199799]
14. Choi G, Huang B, Pinarbasi E, Braunstein SE, Horvai AE, Kogan S, Bhatia S, Faddegon B, Nakamura JL. Genetically mediated Nf1 loss in mice promotes diverse radiation-induced tumors modeling second malignant neoplasms. Cancer Res. 2012;72(24):6425–34. doi: 10.1158/0008-5472.CAN-12-1728. [PubMed: 23071067]
15. Mroue R, Huang B, Braunstein S, Firestone AJ, Nakamura JL. Monoallelic loss of the imprinted gene Grb10 promotes tumor formation in irradiated Nf1+/− mice. PLoS Genet. 2015;11(5):e1005235. doi: 10.1371/journal.pgen.1005235. [PubMed: 26000738]
16. Chao RC, Pyzel U, Fridlyand J, Kuo YM, Teel L, Haaga J, Borowsky A, Horvai A, Kogan SC, Bonifas J, Huey B, Jacks TE, Albertson DG, Shannon KM. Therapy-induced malignant neoplasms in Nf1 mutant mice. Cancer Cell. 2005;8(4):337–48. [PubMed: 16226708]
17. Hobbs GA, Der CJ, Rossman KL. RAS isoforms and mutations in cancer at a glance. J Cell Sci. 2016;129(7):1287–92. doi: 10.1242/jcs.182873. [PubMed: 26985062]
18. Schubbert S, Shannon K, Bollag G. Hyperactive Ras in developmental disorders and cancer. Nat Rev Cancer. 2007;7(4):295–308. doi: 10.1038/nrc2109. [PubMed: 17384584]
19. Weaver KN, Wang D, Cnota J, Gardner N, Stabley D, Sol-Church K, Gripp KW, Witte DP, Bove KE, Hopkin RJ. Early-lethal Costello syndrome due to rare HRAS Tandem Base substitution (c.35_36GC>AA; p.G12E)-associated pulmonary vascular disease. Pediatr Dev Pathol. 2014;17(6):421–30. doi: 10.2350/14-05-1488-OA.1. [PubMed: 25133308]
20. Donnella HJ, Webber JT, Levin RS, Camarda R, Momcilovic O, Bayani N, Shah KN, Korkola JE, Shokat KM, Goga A, Gordan JD, Bandyopadhyay S. Kinome rewiring reveals AURKA limits PI3K-pathway inhibitor efficacy in breast cancer. Nat Chem Biol. 2018;14(8):768–77. doi: 10.1038/s41589-018-0081-9. [PubMed: 29942081]
21. Dienstmann R, Rodon J, Serra V, Tabernero J. Picking the point of inhibition: a comparative review of PI3K/AKT/mTOR pathway inhibitors. Mol Cancer Ther. 2014;13(5):1021–31. doi: 10.1158/1535-7163.MCT-13-0639. [PubMed: 24748656]
22. Sun CM, Xiong DB, Yan Y, Geng J, Liu M, Yao XD. Genetic alteration in phosphofructokinase family promotes growth of muscle-invasive bladder cancer. Int J Biol Markers. 2016;31(3):e286–93. doi: 10.5301/jbm.5000189. [PubMed: 26980488]
23. Matsuda S, Kawamoto K, Miyamoto K, Tsuji A, Yuasa K. PCTK3/CDK18 regulates cell migration and adhesion by negatively modulating FAK activity. Sci Rep. 2017;7:45545. doi: 10.1038/srep45545. [PubMed: 28361970]
24. Wang B, Li Z, Wang C, Chen M, Xiao J, Wu X, Xiao W, Song Y, Wang X. Zygotic G2/M cell cycle arrest induced by ATM/Chk1 activation and DNA repair in mouse embryos fertilized with hydrogen peroxide-treated epididymal mouse sperm. PloS one. 2013;8(9):e73987. doi: 10.1371/journal.pone.0073987. [PubMed: 24040138]
25. Lis P, Dylag M, Niedzwiecka K, Ko YH, Pedersen PL, Goffeau A, Ulaszewski S. The HK2 Dependent “Warburg Effect” and Mitochondrial Oxidative Phosphorylation in Cancer: Targets for Effective Therapy with 3-Bromopyruvate. Molecules. 2016;21(12). doi: 10.3390/molecules21121730.
26. Zhao J, Li J, Fan TWM, Hou SX. Glycolytic reprogramming through PCK2 regulates tumor initiation of prostate cancer cells. Oncotarget. 2017;8(48):83602–18. doi: 10.18632/oncotarget.18787. [PubMed: 29137367]
27. Park JW, Kim SC, Kim WK, Hong JP, Kim KH, Yeo HY, Lee JY, Kim MS, Kim JH, Yang SY, Kim DY, Oh JH, Cho JY, Yoo BC. Expression of phosphoenolpyruvate carboxykinase linked to chemoradiation susceptibility of human colon cancer cells. BMC Cancer. 2014;14:160. doi: 10.1186/1471-2407-14-160. [PubMed: 24602180]

28. Michie AM, Nakagawa R. The link between PKCalpha regulation and cellular transformation. Immunol Lett. 2005;96(2):155–62. doi: 10.1016/j.imlet.2004.08.013. [PubMed: 15585319]

29. Poliakov A, Cotrina ML, Pasini A, Wilkinson DG. Regulation of EphB2 activation and cell repulsion by feedback control of the MAPK pathway. J Cell Biol. 2008;183(5):933–47. doi: 10.1083/jcb.200807151. [PubMed: 19047466]

30. Guo DL, Zhang J, Yuen ST, Tsui WY, Chan AS, Ho C, Ji J, Leung SY, Chen X. Reduced expression of EphB2 that parallels invasion and metastasis in colorectal tumours. Carcinogenesis. 2006;27(3):454–64. doi: 10.1093/carcin/bgi259. [PubMed: 16272170]

31. Pawelczyk T, Matecki A. Localization of phospholipase C delta3 in the cell and regulation of its activity by phospholipids and calcium. Eur J Biochem. 1998;257(1):169–77. [PubMed: 9799116]

32. Vazquez F, Devreotes P. Regulation of PTEN function as a PIP3 gatekeeper through membrane interaction. Cell Cycle. 2006;5(14):1523–7. doi: 10.4161/cc.5.14.3005. [PubMed: 16861931]

33. Kamiya Y, Mizuno S, Komenoi S, Sakai H, Sakane F. Activation of conventional and novel protein kinase C isozymes by different diacylglycerol molecular species. Biochem Biophys Rep. 2016;7:361–6. doi: 10.1016/j.bbrep.2016.07.017. [PubMed: 28955926]

34. Kumar A, Mocklinghoff S, Yumoto F, Jaroszewski L, Farr CL, Grzechnik A, Nguyen P, Weichenberger CX, Chiu HJ, Klock HE, Elsliger MA, Deacon AM, Godzik A, Lesley SA, Conklin BR, Fletterick RJ, Wilson IA. Structure of a novel winged-helix like domain from human NFRKB protein. PloS one. 2012;7(9):e43761. doi: 10.1371/journal.pone.0043761. [PubMed: 22984442]

35. Chen L, Cai Y, Jin J, Florens L, Swanson SK, Washburn MP, Conaway JW, Conaway RC. Subunit organization of the human INO80 chromatin remodeling complex: an evolutionarily conserved core complex catalyzes ATP-dependent nucleosome remodeling. J Biol Chem. 2011;286(13):11283–9. doi: 10.1074/jbc.M111.222505. [PubMed: 21303910]

36. Leung GP, Feng T, Sigoillot FD, Geyer FC, Shirley MD, Ruddy DA, Rakiec DP, Freeman AK, Engelman JA, Jaskelioff M, Stuart DD. Hyperactivation of MAPK Signaling Is Deleterious to RAS/RAF-mutant Melanoma. Mol Cancer Res. 2019;17(1):199–211. doi: 10.1158/1541-7786.MCR-18-0327. [PubMed: 30201825]

37. Long ZJ, Wang LX, Zheng FM, Chen JJ, Luo Y, Tu XX, Lin DJ, Lu G, Liu Q. A novel compound against oncogenic Aurora kinase A overcomes imatinib resistance in chronic myeloid leukemia cells. Int J Oncol. 2015;46(6):2488–96. doi: 10.3892/ijo.2015.2960. [PubMed: 25872528]

38. Wang L, Arras J, Katsha A, Hamdan S, Belkhiri A, Ecsedy J, El-Rifai W. Cisplatin-resistant cancer cells are sensitive to Aurora kinase A inhibition by alisertib. Mol Oncol. 2017;11(8):981–95. doi: 10.1002/1878-0261.12066. [PubMed: 28417568]

39. Sarbassov DD, Guertin DA, Ali SM, Sabatini DM. Phosphorylation and regulation of Akt/PKB by the rictor-mTOR complex. Science. 2005;307(5712):1098–101. doi: 10.1126/science.1106148. [PubMed: 15718470]

40. Sarbassov DD, Ali SM, Sengupta S, Sheen JH, Hsu PP, Bagley AF, Markhard AL, Sabatini DM. Prolonged rapamycin treatment inhibits mTORC2 assembly and Akt/PKB. Mol Cell. 2006;22(2):159–68. doi: 10.1016/j.molcel.2006.03.029. [PubMed: 16603397]

41. Chen XG, Liu F, Song XF, Wang ZH, Dong ZQ, Hu ZQ, Lan RZ, Guan W, Zhou TG, Xu XM, Lei H, Ye ZQ, Peng EJ, Du LH, Zhuang QY. Rapamycin regulates Akt and ERK phosphorylation through mTORC1 and mTORC2 signaling pathways. Mol Carcinog. 2010;49(6):603–10. doi: 10.1002/mc.20628. [PubMed: 20512842]

42. Blakely CM, Watkins TBK, Wu W, Gini B, Chabon JJ, McCoach CE, McGranahan N, Wilson GA, Birkbak NJ, Olivas VR, Rotow J, Maynard A, Wang V, Gubens MA, Banks KC, Lanman RB, Caulin AF, St John J, Cordero AR, Giannikopoulos P, Simmons AD, Mack PC, Gandara DR, Husain H, Doebele RC, Riess JW, Diehn M, Swanton C, Bivona TG. Evolution and clinical impact of co-occurring genetic alterations in advanced-stage EGFR-mutant lung cancers. Nat Genet. 2017;49(12):1693–704. doi: 10.1038/ng.3990. [PubMed: 29106415]

43. Duncan JS, Whittle MC, Nakamura K, Abell AN, Midland AA, Zawistowski JS, Johnson NL, Granger DA, Jordan NV, Darr DB, Usary J, Kuan PF, Smalley DM, Major B, He X, Hoadley KA, Zhou B, Sharpless NE, Perou CM, Kim WY, Gomez SM, Chen X, Jin J, Frye SV, Earp HS, Graves LM, Johnson GL. Dynamic reprogramming of the kinome in response to

targeted MEK inhibition in triple-negative breast cancer. Cell. 2012;149(2):307–21. doi: 10.1016/j.cell.2012.02.053. [PubMed: 22500798]

44. Dobin A, Davis CA, Schlesinger F, Drenkow J, Zaleski C, Jha S, Batut P, Chaisson M, Gingeras TR. STAR: ultrafast universal RNA-seq aligner. Bioinformatics. 2013;29(1):15–21. doi: 10.1093/bioinformatics/bts635. [PubMed: 23104886]
45. Sherborne AL, Lavergne V, Yu K, Lee L, Davidson PR, Mazor T, Smirnoff IV, Horvai AE, Loh M, DuBois SG, Goldsby RE, Neglia JP, Hammond S, Robison LL, Wustrack R, Costello JF, Nakamura AO, Shannon KM, Bhatia S, Nakamura JL. Somatic and Germline TP53 Alterations in Second Malignant Neoplasms from Pediatric Cancer Survivors. Clin Cancer Res. 2017;23(7):1852–61. doi: 10.1158/1078-0432.CCR-16-0610. [PubMed: 27683180]
46. Burgess MR, Hwang E, Mroue R, Bielski CM, Wandler AM, Huang BJ, Firestone AJ, Young A, Lacap JA, Crocker L, Asthana S, Davis EM, Xu J, Akagi K, Le Beau MM, Li Q, Haley B, Stokoe D, Sampath D, Taylor BS, Evangelista M, Shannon K. KRAS Allelic Imbalance Enhances Fitness and Modulates MAP Kinase Dependence in Cancer. Cell. 2017;168(5):817–29 e15. doi: 10.1016/j.cell.2017.01.020. [PubMed: 28215705]
47. Davis S, Charles PD, He L, Mowlds P, Kessler BM, Fischer R. Expanding Proteome Coverage with CHarge Ordered Parallel Ion aNalysis (CHOPIN) Combined with Broad Specificity Proteolysis. J Proteome Res. 2017;16(3):1288–99. doi: 10.1021/acs.jproteome.6b00915. [PubMed: 28164708]

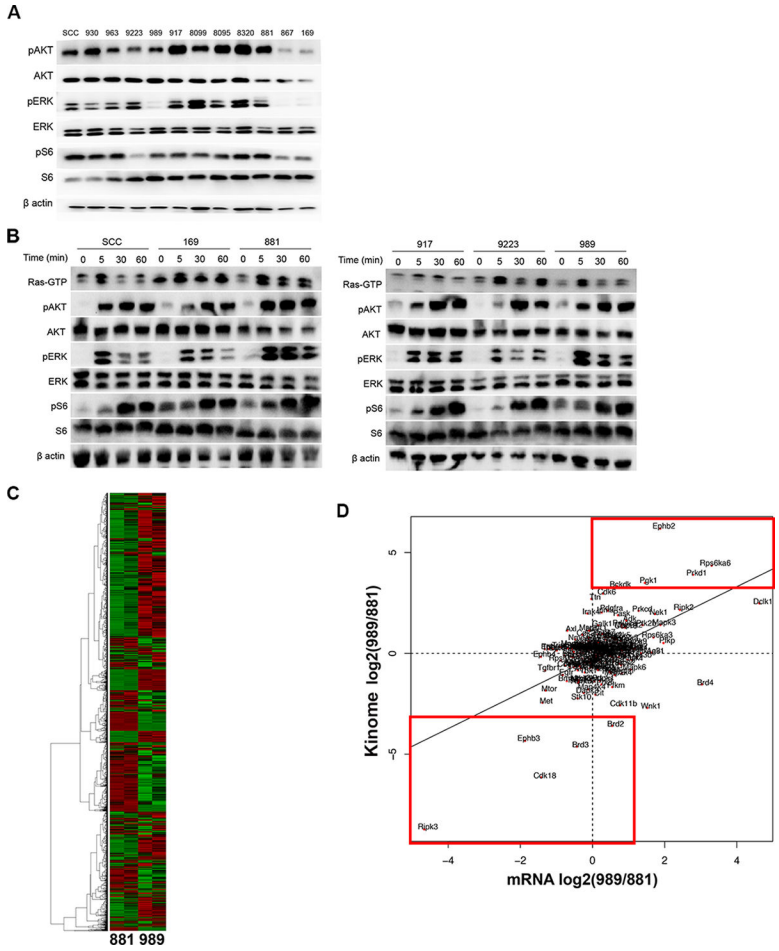

Fig. 1.

Ras signaling among *Nf1* null tumor cell lines. A. Basal Ras signaling was assessed by Western blot analysis. Phosphorylated and total AKT (S473), S6 Ribosomal protein (Ser235/236) and p44/42 MAPK (ERK1/2) (Thr202/Tyr204) in untreated *Nf1* null tumor cell lines shown. β actin was used as loading control. B. RAS activation varies among serum-stimulated *Nf1* null cell lines. *Nf1* null tumor cell lines were serum starved for 24 hours, then stimulated with media containing 10% FBS. Whole cell lysates were collected at 0, 5, 30 and 60 minutes after stimulation and RAS-GTP pull-down was performed. Shown in right panel: Corresponding immunoblotting for phospho-specific antibodies against AKT (S473), S6 (Ser235/236) and p44/42 MAPK (ERK1/2) (Thr202/Tyr204) was assessed. β actin was used as loading control. C. Heat map of transcriptome profiling data shows the unsupervised clustering of analyzed parental cell lines (881 and 989 cell lines, two biological replicates analyzed for both. D. Scatter plots depicting relative expression differences between 989 and 881 cell lines against corresponding relative differences in kinase binding to MIB.

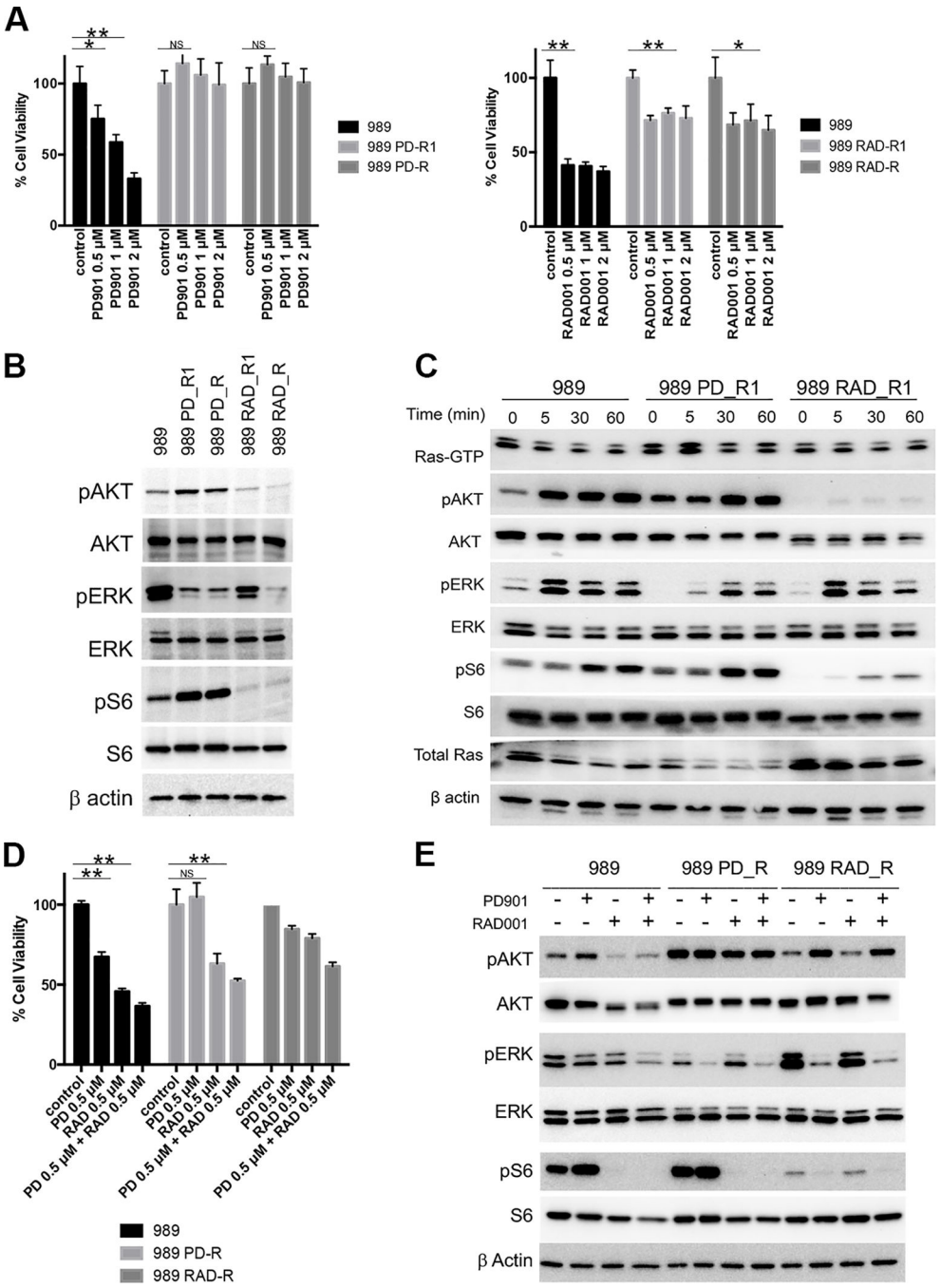

Fig. 2.

Drug resistant 989 *Nf1* mutant cells. A. Two sets of resistant cell lines were derived from 989 parental cells after chronic drug exposure; these were resistant to either 100 nM (989 PD_R1, 989 RAD_R1) or resistant to 500 nM (989 PD_R, 989 RAD_R). Acquired resistance was confirmed by comparing growth by parental and resistant cell lines to increasing concentrations of drug after 72 hours of exposure (*P<0.05; **P<0.01; ns, not significant) by MTS assay. B. Basal Ras signaling in parental and drug resistant derivatives was assessed by Western blotting. Total and phosphorylated AKT (S473), S6 Ribosomal

Protein (Ser235/236) and p44/42 MAPK (ERK1/2) (Thr202/Tyr204) were assessed, with β actin used as loading control. C. After 24 hours of serum starvation, subconfluent cells were stimulated for 0, 5, 30 or 60 minutes with media containing 10% FBS, and protein lysates collected. RAS-GTP levels were assessed by GTPase pull-down. Corresponding immunoblotting for total RAS and phospho-RAS effectors AKT (S473), S6 (Ser235/236) and p44/42 MAPK (ERK1/2) (Thr202/Tyr204) was performed. D. Growth by parental and drug resistant cell lines after 72 hours of exposure to 0.5 μM PD0325901 alone, 0.5 μM RAD001 alone, or the combination was assessed by an MTS assay. Cell viability was assessed after 72 hours of drug exposure (*P<0.05; **P<0.01; ns, not significant). E. Total and phosphorylated AKT (S473), S6 Ribosomal Protein (Ser235/236) and p44/42 MAPK (ERK1/2) (Thr202/Tyr204) in control and drug treated cells were assessed by western blotting.

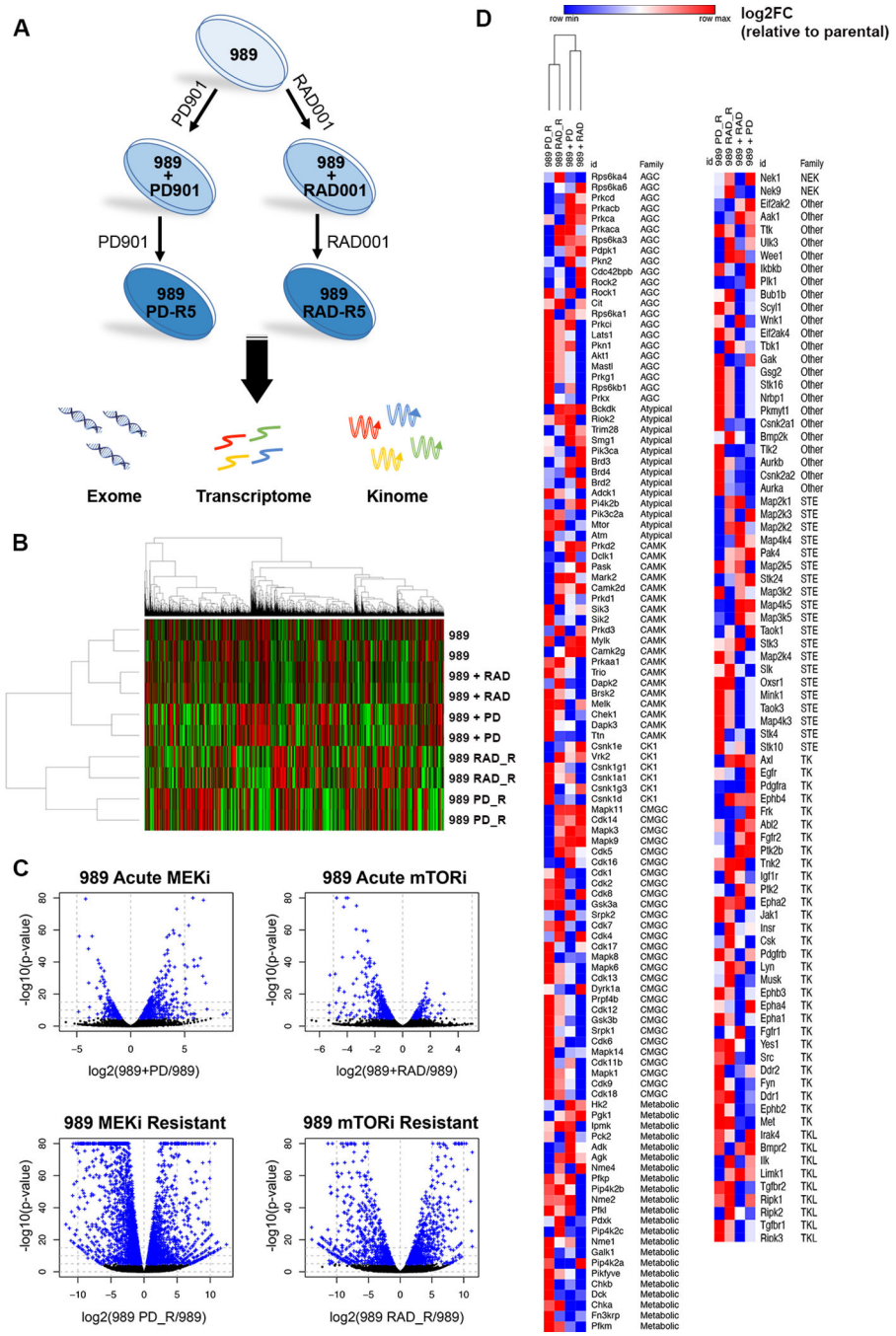

Fig. 3.

Acquired drug resistance in *Nf1* mutant tumor cell lines is associated with remodeled transcriptomes and kinomes. A. Schema describing samples and molecular analysis of parental, acute treated (989+PD901, 989+RAD001) and drug resistant derivatives (989 PD-R5, 989 RAD-R5). B. Heat map depicts unsupervised clustering analysis of transcriptomes of parental and resistant 989 tumor cell lines. Parental and resistant cell lines were grown to a confluence of 70%. Acutely treated parental cell lines (989 + RAD, 989 + PD) were treated with 500 nM PD0325901 or RAD001 for 24 hours. Resistant cells (989 RAD_R,

989 PD_R) were maintained in drug (500 nM) continuously. Drug resistant cells (989 PD_R and 989 RAD_R) cluster together and separately from parental drug-sensitive counterparts (two biological replicates for analyzed for each). C. The upper two panels show log-fold changes in mRNA of acutely drug treated cells relative to parental 989 cells plotted against p-value on the y-axis. Acute (24 hour) exposure to MEKi or mTORi resulted in 774 or 619 genes respectively showing significant expression change compared to parental 989 cells (significantly altered genes are indicated by blue crosses). In contrast, PD resistant and RAD resistant 989 cell lines (relative to parental cells) demonstrate both more genes undergoing expression changes (5133 and 1702 respectively) and greater magnitudes of expression change for significantly altered genes. D. The log2 of LFQ (label free quantification) intensity of each kinase (194 total) was computed and plotted in a heatmap plotting the differences (as compared to control untreated parental cells) in the binding of kinases to MIB by acutely treated (989 + PD, 989 + RAD), PD901- or RAD001-resistant 989 cells (each sample compared to control parental cells). For each experimental condition (acutely treated or drug-resistant), kinase activation or repression in response to 24h treatment with 500 nM PD901 or RAD001 was quantified by subtracting the average Log2LFQs of two biological control replicates (parental cell lines) from the average Log2LFQs of two biological replicates of each experimental group. Red indicates increased MIB binding, blue indicates decreased MIB binding (Kinase families: AGC, Atypical, CAMK, CK1, CMGC, Metabolic, NEK, other, STE, TK, TKL).

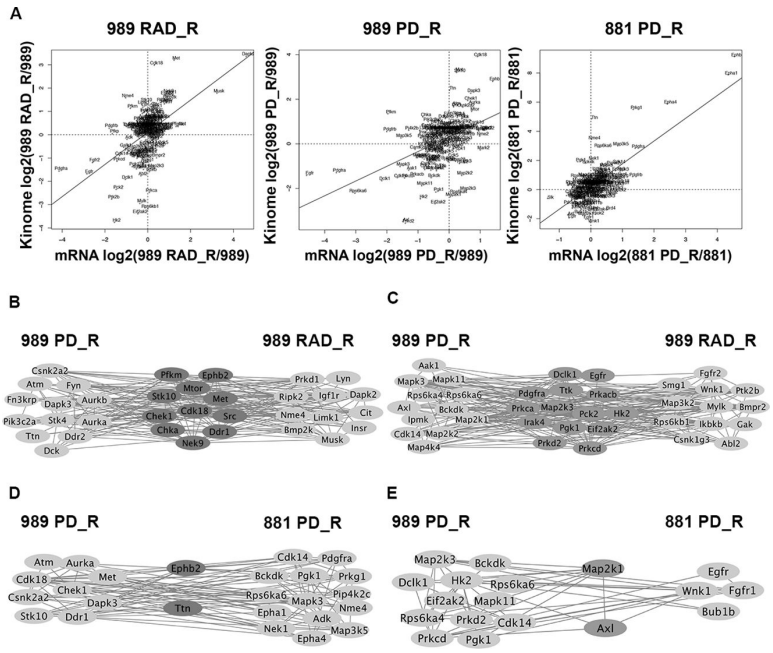

Fig. 4.

Kinome profiles in drug resistant *Nf1* mutant cell lines. A. Scatter plots displaying relative expression differences between drug resistant and parental cells against corresponding relative differences in kinase binding to MIB. B-E. Log2LFQ (label free quantification) intensity of each kinase in parental cells was subtracted from the corresponding Log2LFQ of kinases in drug resistant derivatives. Kinases with Log2LFQ values of >1.5 or <−1.5 were identified, then organized into protein interaction networks using Cytoscape software. Shown in panels B and D are kinases demonstrating increased MIB binding in both 989 PD_R and 989 RAD_R (B) and 989 PD_R and 881 PD_R (D). Shown in panels C and E are kinases demonstrating decreased MIB binding in both 989 PD_R and 989 RAD_R (C) and 989 PD_R and 881 PD_R (E).

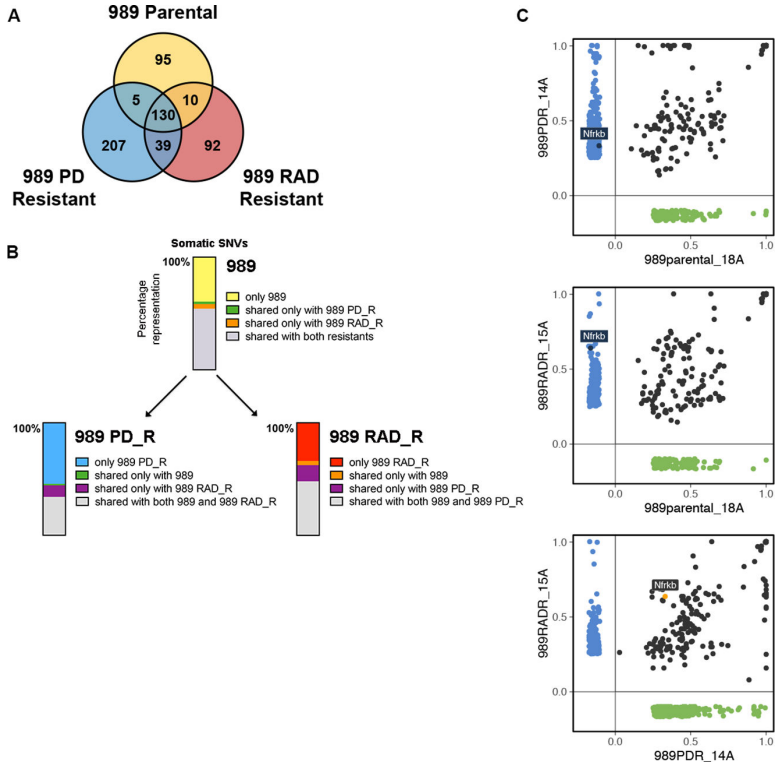

Fig. 5.

Somatic mutations in *Nf1* mutant parental and drug resistant cells. A. The Venn diagram depicts the number of shared and unique somatic SNVs identified in 989, 989 PD_R and 989 RAD_R cell lines. B. The stacked bar graphs depict the private and shared somatic SNVs as percentages of each cell line's total somatic SNVs (normalized, total summing to 100%). Private mutations in 989 PD_R and 989 RAD_R comprised 54.33% and 33.95% of the total somatic SNVs, respectively. C. Variant allele frequency plots comparing *Nf1* mutant 989 parental and drug resistant cell lines. Cell-line specific genes involved by SNVs were highlighted in blue and green. The *Nfrkb* gene was mutated in both resistant 989 PD_R and 989 RAD_R cell lines.

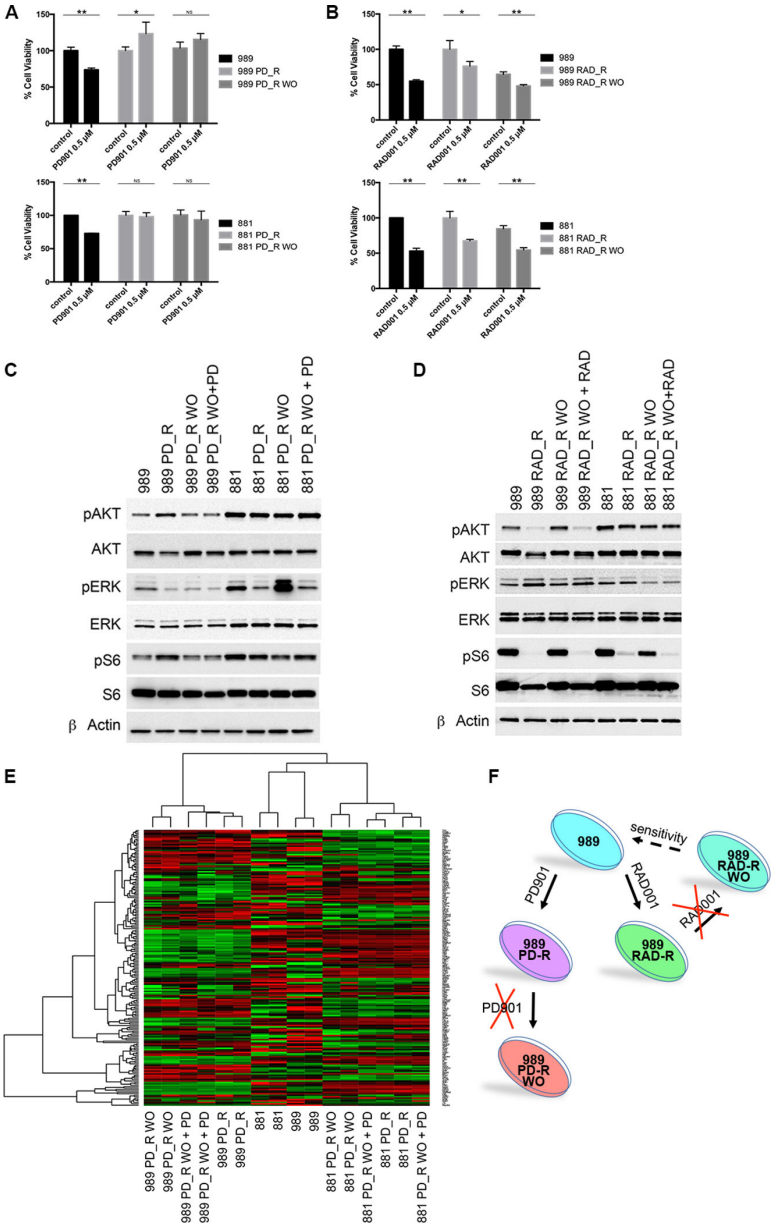

Fig. 6.

Effect of drug withdrawal on drug resistant *Nf1* mutant tumor cells. A-B. Resistant cell lines were washed twice with PBS and then grown drug-free for at least 12 days. Viability of parental, resistant and resistant washout cell lines treated with 0.5 μM PD0325901 or 0.5 μM RAD001 for 72 hours was assessed by MTS proliferation assay. Washout resistant cell lines were normalized to each untreated resistant counterpart (*P<0.05; **P<0.01; ns, not significant). C-D. Western blot analyses were performed to evaluate Ras pathway effector activation in parental, resistant and resistant washout cell lines in response to 24 hours of exposure to either PD0325901 or RAD001. E. Heat map depicts unsupervised clustering analysis of kinase expression in parental and drug resistant 989 and 881 tumor cells (resistant and washout). Drug resistant and washout cells each segregate separately from parental cells but also from each other. F. Schema describing the drug response-based

relationship of drug resistant *Nf1* cell lines to parental cells. Cells chronically treated with PD901 and RAD001 differentiate into new cell lines resistant to the two drugs, 989 PD_R and 989 RAD_R. In response to drug withdrawal, 989 PD_R WO cells progress in the evolution and diverge further from 989 PD_R, whereas 989 RAD_R WO re-sensitize to the drug and revert to the parental state.